Precision Control of the Electron Longitudinal Bunch Shape Using an Emittance-Exchange Beam Line

G. Ha, M. H. Cho, and W. Namkung
POSTECH, Pohang, Gyeongbuk 37673, Republic of Korea

J. G. Power, D. S. Doran, E. E. Wisniewski, M. Conde, W. Gai, W. Liu, C. Whiteford, Q. Gao, K.-J. Kim, A. Zholents, and Y.-E Sun
Argonne National Laboratory, Argonne, Illinois 60439, USA

C. Jing
Euclid TechLabs, Solon, Ohio 44139, USA

P. Piot
Fermi National Accelerator Laboratory, Batavia, Illinois 60510, USA
(Received 19 September 2016; published 9 March 2017)

We report on the experimental generation of relativistic electron bunches with a tunable longitudinal bunch shape. A longitudinal bunch-shaping (LBS) beam line, consisting of a transverse mask followed by a transverse-to-longitudinal emittance exchange (EEX) beam line, is used to tailor the longitudinal bunch shape (or current profile) of the electron bunch. The mask shapes the bunch's horizontal profile, and the EEX beam line converts it to a corresponding longitudinal profile. The Argonne wakefield accelerator rf photoinjector delivers electron bunches into a LBS beam line to generate a variety of longitudinal bunch shapes. The quality of the longitudinal bunch shape is limited by various perturbations in the exchange process. We develop a simple method, based on the incident slope of the bunch, to significantly suppress the perturbations.

DOI: 10.1103/PhysRevLett.118.104801

Precise methods to manipulate the six-dimensional (6D) phase space of high-brightness, relativistic electron bunches are attracting increasing attention. This interest is being driven by the awareness that the next generation of electron linear accelerator applications (e.g., a future linear collider or x-ray light sources [1–3]) will demand unprecedented control over both the beam's transverse and longitudinal phase space.

Manipulation in transverse phase space is straightforward through the use of multipole magnets (e.g., quadrupoles), collimators, etc. Longitudinal phase-space manipulation is considerably more difficult to achieve. While it is straightforward to manipulate the momentum with an accelerating cavity, the longitudinal distribution of particles within the bunch is difficult to control due to the short duration of the typical high-brightness electron bunch (subpicosecond to tens of picosecond scale). Thus, longitudinal bunch shaping has remained elusive until the past decade where a few different methods have been suggested [4–10].

There are many electron linac-based applications that would benefit from precisely tailored longitudinal bunch shapes. These include superradiant radiation [11–13], beam quality control for a high-brightness beam [14–18], seeding techniques to enhance the performances of the x-ray free electron laser [19–21], and improving the efficiency of ultrahigh-gradient wakefield accelerations [22–24].

Longitudinal bunch shaping has become an active area of research and development in recent years due, in part, to the recent progress in accurate simulations and precise experimental methods. There are two fundamental approaches that can be taken to manipulate the longitudinal bunch shape: correlation-based and exchange-based methods. The former method introduces a temporary correlation between the longitudinal position (z) and another coordinate which is easier to control [e.g., the horizontal position (x) or the fractional momentum deviation (δ)]. Once the correlation is established, the bunch distribution is manipulated along the other coordinate (e.g., by using a collimator), and the correlation is finally removed. Thus, these approaches indirectly control the longitudinal distribution by manipulating another coordinate as exemplified in Refs. [4,5].

In this Letter, we present the first experimental demonstration of an alternative bunch-shaping technique based on a phase-space exchange scheme [6] that employs a transverse-to-longitudinal emittance exchange (EEX) beam line [1,25,26]. Instead of introducing a correlation, this method exchanges the horizontal (x, x') and longitudinal (z, δ) phase-space coordinates. Consequently, any features introduced in the horizontal phase space can be transferred to the longitudinal phase space. The advantage of this method is that the mature techniques of transverse phase-space manipulation can be used to control the longitudinal bunch shape. Thus, in principle, the exchange-based method is capable of realizing arbitrary control over the longitudinal bunch shape [6].

There are several different beam line configurations [27,28] that can exchange the horizontal and longitudinal emittance, as long as the beam line satisfies the general EEX condition [29]. We used the double dogleg EEX beam line, since it has the simplest form, making it an ideal candidate for understanding the fundamental beam dynamics of the bunch-shaping process. The double dogleg EEX beam line consists of two identical doglegs each with dispersion η and a transverse deflecting cavity (TDC) of normalized kick strength κ, where $\kappa = (eV/pc)(2\pi/\lambda)$ (e is the electronic charge, pc is the mean momentum, V is the deflecting voltage, and λ is the rf wavelength), in between the doglegs (Fig. 1). For this beam line, the EEX condition is $1 + \kappa\eta = 0$. This is the condition that produces the zero-diagonal elements in the transfer matrix for (x, x', z, δ) phase space [1]. The exchange process can be fully described in 4D phase space via the linear transfer matrix

$$M_{\mathrm{EEX}} = \begin{pmatrix} 0 & 0 & \kappa(L+L_D) & \eta+\kappa\xi(L+L_D) \\ 0 & 0 & \kappa & \kappa\xi \\ \kappa\xi & \eta+\kappa\xi(L+L_D) & 0 & 0 \\ \kappa & \kappa(L+L_D) & 0 & 0 \end{pmatrix}, \quad (1)$$

where $L = 2L_B/\cos(\alpha) + L_{DL}/\cos^2(\alpha)$, $\eta = 2L_B[\cos(\alpha) - 1]/\sin(\alpha)\cos(\alpha) - L_{DL}\sin(\alpha)/\cos^2(\alpha)$, $\xi = L_{DL}\sin^2(\alpha)/\cos^2(\alpha) + 2L_B/\cos(\alpha) - 2L_B\alpha/\sin(\alpha)$, L_B is the length of dipole, α is the bending angle, L_{DL} is the length between dipoles (B-to-B), and L_D is the length between the dipole and TDC [30]. In this equation, we used rectangular dipole magnets and the thin-lens approximation of the TDC to calculate the transfer matrix.

Since the diagonal 2×2 blocks in the transfer matrix are zero, the final longitudinal coordinates (z_f, δ_f) solely depend on the incoming horizontal coordinates (x_i, x_i') and vice versa.

Additionally, the relationship between z_f and x_i can be further simplified to

$$z_f = \{\kappa\xi + S[\eta + \kappa\xi(L + L_D)]\}x_i, \quad (2)$$

where $S \equiv dx'/dx|_{x=0}$ is the slope of the initial phase space [31] and κ and η satisfy the EEX condition. According to Eq. (2), any initial horizontal density profile can be mapped to the final longitudinal density profile. A transverse mask was used to tailor the horizontal profile due to its simplicity. Given the interceptive nature of such a mask, the implementation of the proposed bunch-shaping technique in high-energy or high-repetition accelerators would have to be performed at low energies where beam losses can be tolerated.

The longitudinal bunch-shaping experiment was performed at the Argonne wakefield accelerator facility [32] and is diagrammed in Fig. 1. It consists of the following four sections: (i) the rf photoinjector, (ii) the transverse manipulation beam line, (iii) the EEX beam line, and (iv) the main diagnostic beam line.

In the L-band 1.5 cell rf photoinjector, a 5-nC, 8-MeV electron bunch was generated and further accelerated through the linear accelerator (linac) to a final energy of 48 MeV. The electron bunch phase is normally set to on crest (0°) in the cavities but can be adjusted in order to control the longitudinal slope (i.e., chirp). (A negative phase reduces the energy of the head and increases the energy of the tail.)

The transverse manipulation beam line included four quadrupole magnets and a series of selectable 100-micron-thick tungsten masks. The quadrupole magnets controlled the size and slope of the horizontal and vertical phase ellipse. Each transverse mask generated a different initial horizontal profile [33] by scattering the unwanted portion of the beam. The initial horizontal bunch profile was measured with a YAG screen located in the straight ahead line (YAG1).

The EEX beam line used rectangular dipole magnets (B) to bend the electron bunch by 20°. Each dogleg generated a horizontal dispersion of $\eta_x \cong 0.9$ m and a momentum compaction factor of $\xi \cong 0.3$ m [34]. The L-band TDC in the middle of the EEX beam line (TDC1) consists of three cells [35]. The power applied to TDC1 was adjusted to satisfy the EEX condition $1 + \kappa\eta = 0$.

In the main diagnostic beam line, located after the EEX beam line, three quadrupole magnets and a TDC were installed along with YAG screens both upstream (YAG2) and downstream (YAG3) of TDC2. During its nominal operation (5 MW input power), TDC2 can resolve the bunch longitudinal profile with a resolution of less than 30 μm.

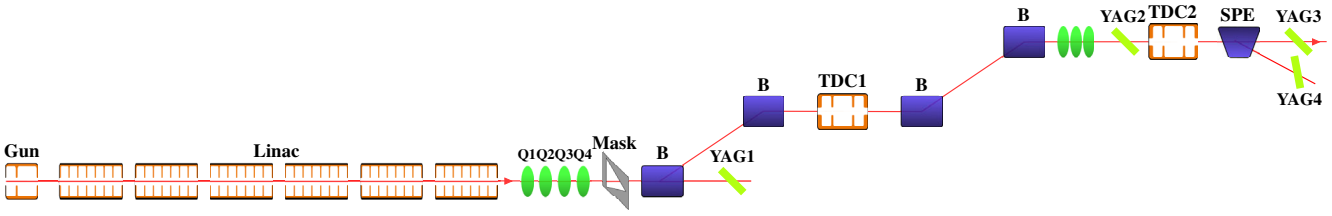

FIG. 1. Schematic diagram of the experimental beam. The acronyms Q, B, TDC, and SPE stand for the quadrupole magnet, dipole magnet, transverse deflecting cavity, and spectrometer, respectively. Dipole magnets and TDC1 bend or kick the beam horizontally, and TDC2 kicks the beam vertically.

The first set of experiments focused on demonstrating the longitudinal bunch-shaping capabilities of the exchange-based method (see Fig. 2). The top row of Fig. 2 shows transverse bunch images at YAG1 without a mask (a) and with several different masks (b)–(e). The total charge before the mask was ~5 nC, which was reduced after the mask to ~1–1.5 nC depending on the mask used. The electron bunch had an approximately symmetric horizontal profile before the mask (a) and was converted into two rectangular-shaped transverse beamlets (b), a triangle (c), a rectangle (d), and a trapezoid (e). These transversely shaped electron bunches were transported through the EEX beam line, and their final longitudinal density profiles were measured with TDC2 at YAG3.

The bottom row of Fig. 2 shows the longitudinal bunch shapes measured at YAG3 (g)–(j) that corresponds to the horizontal bunch shapes in the top row. As can be seen, the final longitudinal bunch shapes closely follow the corresponding initial horizontal bunch shapes. We observe a longitudinally separated two-bunch train (g), a triangle (h), a rectangle (i), and a trapezoid (j).

The bottom row of Fig. 2 also shows the final horizontal distribution of the bunch which is determined by its initial longitudinal features. The final horizontal bunch shapes in Figs. 2(f)–2(j) retain none of their initial horizontal shape from the mask. Instead, all of the horizontal distributions show a similar asymmetric pattern, brighter on the top and dimmer on the bottom, due to a weak transverse-longitudinal correlation before the mask. The slight difference in the asymmetric patterns between (g) and (h) is because the different masks cut the initial profiles in different ways.

While this Letter is focused on the final longitudinal bunch shape, we note that all of the other final beam properties at the exit of the EEX beam line can be controlled. Final transverse properties are controlled with quadrupoles after the EEX beam line, and final longitudinal properties can be controlled with quadrupoles before the first EEX dipole. An experiment is planned that will use this beam line to create a drive and witness beam and make them pass through a dielectric structure with a small aperture to achieve a high transformer ratio [36]. The only limitation of this beam line is that the final horizontal emittance is large (due to the initial longitudinal emittance), but this can be overcome with a double EEX beam line [14].

The second experimental result we present is the first demonstration of a new perturbation suppression method that we term the slope-control method.

Equations (1) and (2) imply perfect conversion from the horizontal to the longitudinal shape. In reality, these equations ignore important perturbations including finite bunch emittance, the thick-lens effect of the TDC, second-order effects, and collective effects [37,38]. These perturbations distort the ideal longitudinal bunch shape, as can be clearly seen by comparing Figs. 2(b) and 2(g). Each horizontal beamlet produced by the two-slit mask has a sharp, rectanglelike shape [Fig. 2(b)]. According to Eqs. (1) and (2), the longitudinal bunch train should have the same rectangular shape, but the sharp features of the profile are smeared [Fig. 2(g)] due to the aforementioned perturbations.

Previous researchers have studied several different types of linear perturbations that arise in the EEX beam line and have proposed several methods to suppress them [14,25,38]. In our previous theoretical work [39], we derived analytic

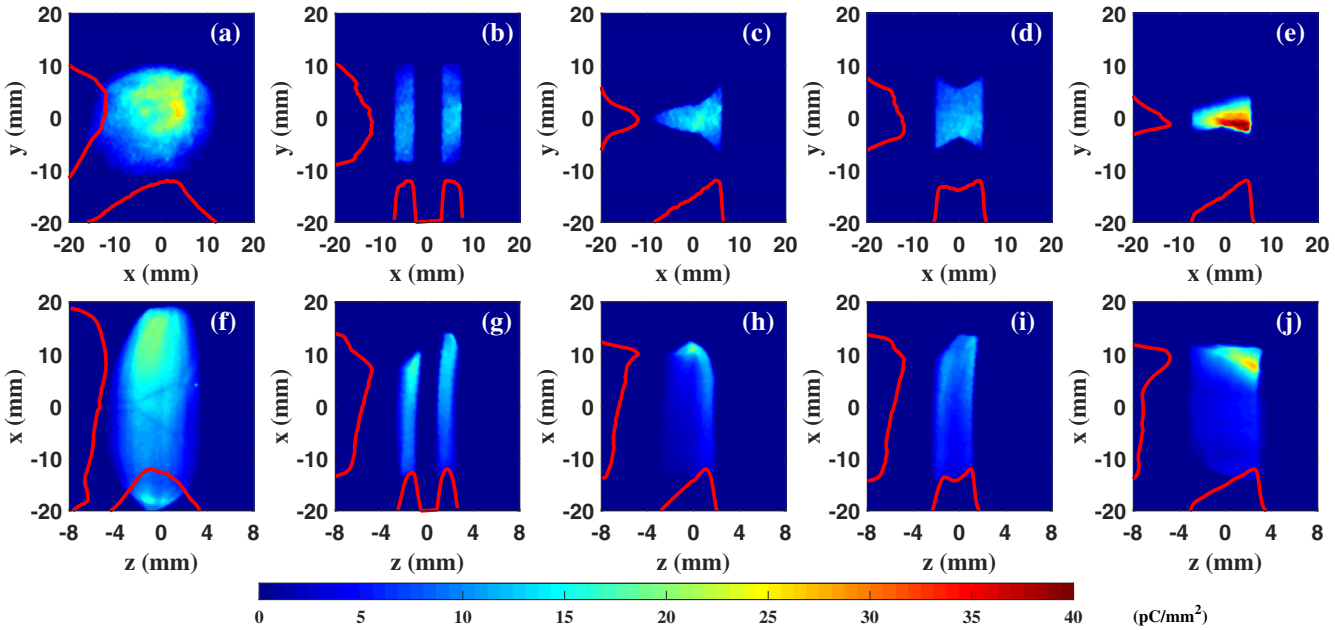

FIG. 2. Electron beam images at YAG1 with different masks (a)–(e) and corresponding beam images at YAG3 with TDC2 on. The x axis of images (f)–(j) is rescaled based on the TDC2 calibration. The red traces are the corresponding projections.

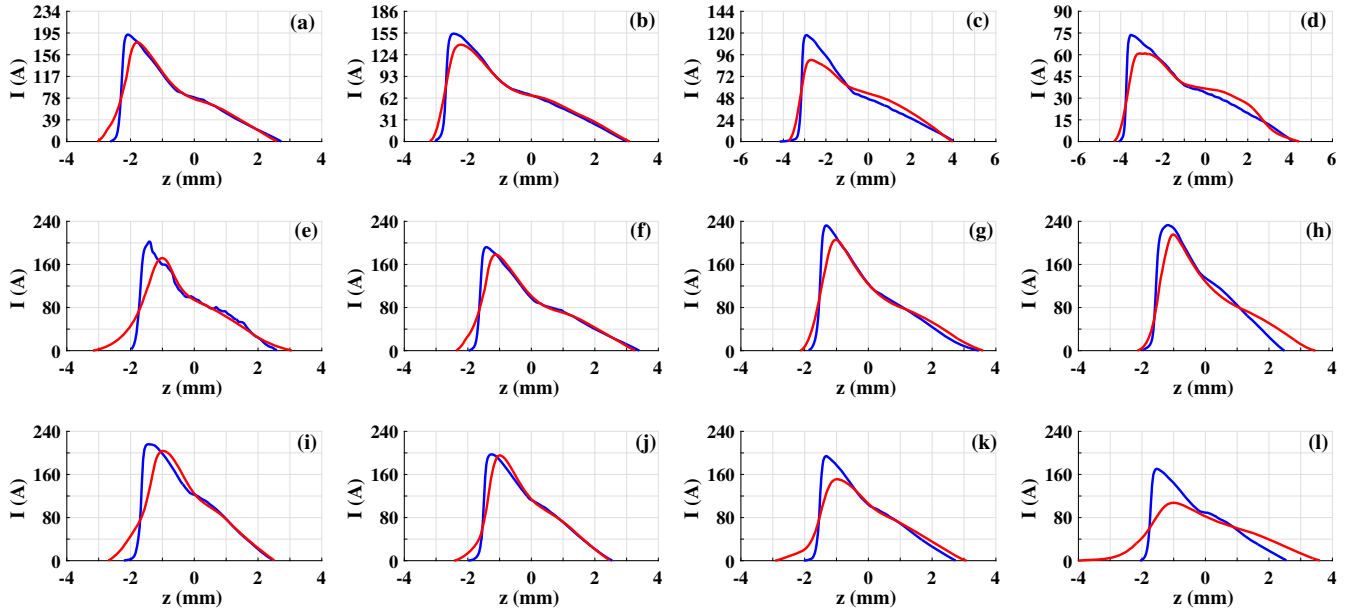

FIG. 3. Horizontal density profiles measured at YAG1 with the first EEX dipole off (blue curve) and longitudinal density profiles measured at YAG3 with TDC2 on (red curve). The base lines for horizontal and vertical slopes were zero, and the linac phase was −15°. Each setting was fixed to the base line while one of them was scanned. Horizontal slopes of the incoming electron beam were 0.0, 0.2, 0.4, and 0.6 m^{-1} for (a)–(d). Vertical slopes were −0.6, 0.0, 0.2, and 0.6 m^{-1} for (e)–(h). The linac phase which controls the longitudinal chirp was −10°, −15°, −25°, and −40° for (i)–(l). Here the tail of the profile indicates the peak to the left end of the profile.

expressions for both linear and nonlinear perturbations, and, furthermore, we developed a new method to suppress them termed the "slope-control method."

The slope-control method adjusts the three incoming slopes, in the x, y, and z phase spaces, to partially suppress the perturbations due to the linear thick-lens effect as well as the nonlinear effects: second-order terms and collective effects due to space-charge (SC) and coherent synchrotron radiation (CSR). As an example, the perturbation due to the horizontal second-order terms was shown in Ref. [39] to be given by the expression $\Delta z_f \approx Ax_0^2 + Bx_0x_0' + Cx_0'^2$. This perturbation can be minimized by taking the partial derivative of it with respect the slope of the incident bunch $(\langle x_i x_i' \rangle / \langle x_i^2 \rangle)$, in which case the minimizing slope before the mask is $-A/2C$. In general, the slope-control method is powerful and simple, since it can suppress nonlinear perturbations and does not require any significant modification to the beam line. In our experiment, the bunch length was ∼10 ps, and the slope-control method worked well for our range of parameters.

During the experiment, the linac (Fig. 1) phase was used to control the longitudinal slope (i.e., chirp), and the four quadrupoles (Q1–Q4 in Fig. 1) in front of the EEX beam line were used to control both the horizontal and vertical bunch sizes and slopes at the mask.

To demonstrate the slope-control method, the longitudinal bunch shape was monitored while the three slopes were varied. The optimal values of the slopes are defined as the values of slopes chosen to suppress the perturbations. The optimal values were calculated [39] to be −0.27 m^{-1} for the horizontal, 0.13 m^{-1} for the vertical, and a linac phase of −15°. During the experiment, the values of the slopes were varied about the base values that we define as 0.0 m^{-1} for the horizontal and vertical slopes and a linac phase of −15°, since these are the values the rf photoinjector is typically operated and it is hard to sustain the transverse slope exactly at the optimal values with different rf phases.

The experimental values of the transverse slopes were calculated from the measurement of the beam sizes at the mask position (YAG screen not shown) and YAG1 (Fig. 1). This value is an approximation of the conventional slope and therefore has a small error [31]. The experimental value of the longitudinal chirp was inferred from the linac phase measurement.

Figure 3 shows the experimental data of the initial horizontal profile measured at YAG1 (blue curve) and the final longitudinal profile measured at YAG3 (red curve) for different transverse slopes and linac phase settings. The horizontal profile is scaled using the transfer matrix to convert it to the ideal longitudinal profile. Ideally, these profiles would be identical.

The effect of the horizontal slope on perturbation suppression is shown in the top row of Fig. 3. The four profiles (a)–(d) correspond to incoming horizontal slopes of $\{0.0, +0.2, +0.4, +0.6\}$ m^{-1}. Note that, for the slopes of both 0.0 m^{-1} and +0.2 cm^{-1}, the initial horizontal profile and final longitudinal profile show good agreement. However, the head (right side) of the beam has a convex curvature as the

horizontal slope increases, while the tail length, from the peak to the left end of the profile, stays approximately 1 mm. This is in good agreement with the analytically predicted slope needed to suppress the perturbations [39].

With the horizontal slope fixed at $0.0\,\mathrm{m}^{-1}$, the effect of the vertical slope on perturbation suppression is shown in the middle row of Fig. 3. The four profiles (e)–(h) correspond to the incoming vertical slopes of $\{-0.6, 0.0, +0.2, +0.6\}$ m^{-1}. Again, both the 0.0 and $+0.2$ m^{-1} cases show good agreement between the initial and final profiles. Each extreme slope case shows significant perturbations in which electrons are shifted towards the head or the tail. This perturbation pattern also shows reasonable agreement with the analytically predicted pattern from the vertical second-order terms given in Ref. [39].

The effect of the longitudinal chirp on the perturbation suppression is shown in the last row of Fig. 3 and the chirp controls three limiting factors at the same time. The thick-lens effect and the second-order effect can be minimized with the chirp of $-1/\xi$ [25,39]. Unfortunately, this chirp also minimizes the bunch length before the second dogleg, so it results in a strong SC or CSR effect on the shaped longitudinal profile [37]. The four profiles (i)–(l) correspond to the linac phase of $\{-10°, -15°, -25°, -40°\}$. Compared with the base phase $-15°$, the phase $-10°$ generates a longer tail, while the head of the profile still has a reasonable agreement with the initial profile. Because of the single triangle profile, the perturbation from the thick-lens effect mostly changes the tail length. However, the $-25°$ case makes a longer tail and changes the head simultaneously. In this case, CSR dominates the perturbation on the profile. Thus, it makes the overall bunch length longer than expected. The same patterns become even clearer at $-40°$.

Overall, the measurements (Fig. 3) are in reasonable agreement with the predicted slopes.

In summary, we experimentally demonstrated the ability of the phase-space-exchange method to form arbitrarily shaped longitudinal profiles. We also validated a simple aberration-control scheme that circumvents possible limitations of the technique. These experimental results confirm the power and versatility of the phase-space exchange-based shaping technique and should prove useful to advance beam-driven acceleration techniques, accelerator-based light sources, and a wide range of future electron linac applications.

This work is supported by POSTECH and Department of Energy, Office of High Energy Physics, under Contract No. DE-AC02-06CH11357.

[1] P. Emma, Z. Huang, K.-J. Kim, and P. Piot, Phys. Rev. Accel. Beams **9**, 100702 (2006).
[2] R. Brinkmann, Y. Derbenev, and K. Flottmann, Phys. Rev. Accel. Beams **4**, 053501 (2001).
[3] C. Feng, T. Zhang, H. Deng, and Z. Zhao, Phys. Rev. Accel. Beams **17**, 070701 (2014).
[4] P. Muggli, B. Allen, V. E. Yakimenko, J. Park, M. Babzien, K. P. Kusche, and W. D. Kimura, Phys. Rev. Accel. Beams **13**, 052803 (2010).
[5] P. Piot, C. Behrens, C. Gerth, M. Dohlus, F. Lemery, D. Mihalcea, P. Stoltz, and M. Vogt, Phys. Rev. Lett. **108**, 034801 (2012).
[6] P. Piot, Y.-E Sun, J. G. Power, and M. Rihaoui, Phys. Rev. Accel. Beams **14**, 022801 (2011).
[7] R. J. England, J. B. Rosenzweig, and G. Travish, Phys. Rev. Lett. **100**, 214802 (2008).
[8] F. Lemery and P. Piot, Phys. Rev. Accel. Beams **18**, 081301 (2015).
[9] C. Jing, J. G. Power, M. Conde, W. Liu, Z. Yusof, A. Kanareykin, and W. Gai, Phys. Rev. Accel. Beams **14**, 021302 (2011).
[10] G. Penco, M. Danailov, A. Demidovich, E. Allaria, G. DeNinno, S. DiMitri, W. M. Fawley, E. Ferrari, L. Giannessi, and M. Trovo, Phys. Rev. Lett. **112**, 044801 (2014).
[11] A. Halperin, A. Gover, and A. Yariv, Phys. Rev. A **50**, 3316 (1994).
[12] S. E. Korbly, A. S. Kesar, J. R. Sirigiri, and R. J. Temkin, Phys. Rev. Lett. **94**, 054803 (2005).
[13] S. Antipov, M. Babzien, C. Jing, M. Fedurin, W. Gai, A. Kanareykin, K. Kusche, V. Yakimenko, and A. Zholents, Phys. Rev. Lett. **111**, 134802 (2013).
[14] A. A. Zholents and M. S. Zolotorev, Report No. ANL-APS-LS-327, 2011.
[15] B. E. Carlsten, K. A. Bishofberger, S. J. Russell, and N. A. Yampolsky, Phys. Rev. Accel. Beams **14**, 084403 (2011).
[16] S. Antipov, S. Baturin, C. Jing, M. Fedurin, A. Kanareykin, C. Swinson, P. Schoessow, W. Gai, and A. Zholents, Phys. Rev. Lett. **112**, 114801 (2014).
[17] A. Zholents *et al.*, Nucl. Instrum. Methods Phys. Res., Sect. A **829**, 190 (2016).
[18] C. Mitchell, J. Qiang, and P. Emma, Phys. Rev. Accel. Beams **16**, 060703 (2013).
[19] L.-H. Yu *et al.*, Science **289**, 932 (2000).
[20] D. Xiang and G. Stupakov, Phys. Rev. Accel. Beams **12**, 030702 (2009).
[21] B. Jiang, J. G. Power, R. Lindberg, W. Liu, and W. Gai, Phys. Rev. Lett. **106**, 114801 (2011).
[22] C. Jing, A. Kanareykin, J. G. Power, M. Conde, Z. Yusof, P. Schoessow, and W. Gai, Phys. Rev. Lett. **98**, 144801 (2007).
[23] B. Jiang, C. Jing, P. Schoessow, J. Power, and W. Gai, Phys. Rev. Accel. Beams **15**, 011301 (2012).
[24] M. Tzoufras, W. Lu, F. S. Tsung, C. Huang, W. B. Mori, T. Katsouleas, J. Vieira, R. A. Fonseca, and L. O. Silva, Phys. Rev. Lett. **101**, 145002 (2008).
[25] M. Cornacchia and P. Emma, Phys. Rev. Accel. Beams **5**, 084001 (2002).
[26] Y.-E. Sun, P. Piot, A. Johnson, A. H. Lumpkin, T. J. Maxwell, J. Ruan, and R. Thurman-Keup, Phys. Rev. Lett. **105**, 234801 (2010).
[27] D. Xiang and A. Chao, Phys. Rev. Accel. Beams **14**, 114001 (2011).

[28] C. R. Prokop *et al.*, in *Proceedings of the 4th International Particle Accelerator Conference, IPAC-2013, Shanghai, China, 2013* (JACoW, Geneva, 2013), p. 3103.
[29] R. P. Fliller, III, Fermi Beams-doc-2553, 2006.
[30] Y.-E Sun *et al.*, in *Proceedings of the 22nd Particle Accelerator Conference, PAC-2007, Albuquerque, NM, 2007* (IEEE, New York, 2007), p. 3441.
[31] A. W. Chao, K. H. Mess, M. Tigner, and F. Zimmermann, *Handbook of Accelerator Physics and Engineering* (World Scientific, Singapore, 2013).
[32] M. Conde *et al.*, in *Proceedings of the 27th Particle Accelerator Conference, Richmond, VA, 2015* (JACoW, Geneva, 2015), p. 2472.
[33] J. G. Power *et al.*, in *Proceedings of the 2014 International Particle Accelerator Conference, Dresden, Germany, 2014* (JACoW, Geneva, 2014), p. 1506.
[34] G. Ha *et al.*, in *Proceedings of the 2015 International Particle Accelerator Conference, Richmond, VA, 2015* (JACoW, Geneva, 2015), p. 2575.
[35] M. Conde *et al.*, in *Proceedings of the 3rd International Particle Accelerator Conference, New Orleans, LA, 2012* (IEEE, Piscataway, NJ, 2012), p. 3350.
[36] Q. Gao *et al.*, in *Proceedings of the 2016 North America Particle Accelerator Conference, Chicago, IL, 2016* (JACoW, Geneva, 2016), p. THPOA08.
[37] G. Ha *et al.*, *AIP Conf. Proc.* 1507, 693 (2012).
[38] D. Y. Shchegolkov and E. I. Simakov, Phys. Rev. Accel. Beams **17**, 041301 (2014).
[39] G. Ha, M. H. Cho, W. Gai, K.-J. Kim, W. Namkung, and J. G. Power, Phys. Rev. Accel. Beams **19**, 121301 (2016).